Ba-Doped $BiFeO_3$ Nanomaterials Synthesized via Sol-Gel Auto-Combustion: Structural, Dielectric, Ferroelectric, and Magnetic Properties

Muhammad Junaid Khan[1], Tanvir Hussain[1], Umar Asim[2], Muhammad Madni[2], Ghulam Asghar[3]

[1]Department of Physics, University of Management and Technology, Lahore, Pakistan.
[2]Institute of Chemical Sciences, Bahauddin Zakariya University, Multan, Punjab, Pakistan.
[3]Interdisciplinary Research Center for Hydrogen Technologies and Carbon Management, King Fahd University of Petroleum and Minerals, Dhahran, Saudi Arabia

Abstract: $BiFeO_3$ is a unique room-temperature multiferroic material exhibiting both ferroelectric and antiferromagnetic ordering, but its applications are limited by weak magnetic properties and high leakage currents. In this study, Ba-doped $BiFeO_3$ nanomaterials with compositions $Ba_xBi_{1-x}FeO_3$ (x = 0.0, 0.10, 0.20, 0.25, 0.30) were synthesized via the sol-gel auto-combustion method to enhance multiferroic performance. X-ray diffraction confirmed a rhombohedral perovskite structure with minor secondary phases, while Ba doping induced lattice distortion, reduced crystallite size, and increased strain. Dielectric measurements showed a progressive increase in dielectric constant and reduced dielectric loss with higher Ba content, attributed to improved polarization and suppressed leakage. Ferroelectric (P–E) loops exhibited enhanced remanent polarization and improved loop squareness, indicating better domain alignment and lower conductivity. Magnetic (M–H) hysteresis loops revealed significant enhancement in remanent and saturation magnetization with increasing Ba concentration, due to spin cycloid suppression and the presence of uncompensated surface spins. These results demonstrate that Ba substitution is an effective route to tailor the structure and enhance the multifunctional properties of $BiFeO_3$ nanomaterials. The improved multiferroic behavior makes them strong candidates for applications in spintronic devices, magnetoelectric sensors, and multifunctional nanoelectronics.

Keywords: Mliferroics, Ba-Doping, Dielectric Properties, Ferroelectric Polarization, Magnetization Enhancement, Sol-Gel Auto-Combustion, XRD Analysis, Nanoscale Materials, P-E Loops, M-H Loops
Email: engrumarasim@yahoo.com

1. Introduction

Multiferroic materials, exhibiting the simultaneous presence of ferrelectric and ferromagnetic properties, are at the forefront of materials science due to their potential for revolutionary applications in energy-efficient electronics, memory devices, and sensors [1, 2]. The intrinsic coupling of these properties can lead to enhanced functionality, enabling the development of multifunctional devices that respond to both electric and magnetic fields. This coupling is especially significant in the emerging field of spintronics, where it can be harnessed to create novel data storage soulutions, and in the development of next-generation computing technologies [3, 4]. The classification of multiferroics into type-I and type-II systems underscores the diversity in their properties and coupling mechanisms. Type-I multiferroics, like $BiFeO_3$, exhibit both ferroelectricity and ferromagnetism, but the coupling between these properties remains weak. In contrast, type-II multiferroics show stronger coupling, typically driven by magnetic ordering that

induces ferroelectricity. However, the relatively low magnetoelectric (ME) coupling in type-I materials such as $BiFeO_3$ limits their practical application in advanced electronic devices [5].

Bismuth ferrite ($BiFeO_3$), a prominent type-I multiferroic, stands out due to its room temperature ferroelectric and weak ferromagnetic properties. Despite its impressive Curie temperature (Tc ≈1043 K) and Neel temperature (Tn ≈ 647 K), BiFeO3 suffers from low polarization and magnetization, limiting its potential in high-performance devices. Additionally, the weak coupling between its electric and magnetic orders has hindered its application in spintronics and other memory technologies. Thus, enhancing the ferroelectric, ferromagnetic, and ME properties of $BiFeO_3$ is crucial for unlocking its full potential [6]. The unique ferroelectric behavior of $BiFeO_3$ is attributed to the off-center displacement of the Bi^{3+} ions in the perovskite lattice, which leads to a spontaneous dipole moment. The weak ferromagnetism, on the other hand, arises from the g-type antiferromagnetic ordering of Fe^{3+} spins, which can be canted to give rise to a net magnetization. While these properties make $BiFeO_3$ a promising candidate for multiferroic applications, its weak ME coupling and low polarization and magnetization need to be addressed for practical usage [7, 8]. Moreover, the spontaneous polarization of $BiFeO_3$ is hindered by the spin cycloid structure, which prevents the material from achieving the maximal ferroelectric response at room temperature. In addition, the weak ferromagnetic moment due to the canting of Fe spins limits its effectiveness in applications requiring strong magnetization [9]. Therefore, developing strategies to enhance both the ferroelectric and ferromagnetic properties is an ongoing challenge in multiferroic research.

Doping has emerged as one of the most effective strategies for enhancing the properties of $BiFeO_3$. Substituting ions with larger ionic radii into the crystal lattice of $BiFeO_3$ can induce structural distortions, leading to enhanced polarization and magnetization. Ba^{2+} ions, with an ionic radius of 1.38 Å, are particularly attractive dopants due to their ability to increase the lattice distortion by replacing smaller Bi^{3+} ions (1.03 Å). This results in an increased off-centering displacement of the Bi^{3+} ions, thereby enhancing the ferroelectric properties. Furthermore, Ba doping can induce changes in the magnetic structure of $BiFeO_3$, promoting canting of the Fe spins and improving its net magnetization [10, 11]. Ba doping has been extensively studied in $BiFeO_3$, with research indicating that even small amounts of Ba can significantly improve both the ferroelectric and ferromagnetic properties. For instance, the introduction of Ba2+ has been shown to suppress the spin cycloid structure in $BiFeO_3$, leading to enhanced magnetization and polarization. These findings suggest that Ba-doped $BiFeO_3$ could be a promising candidate for applications in spintronic devices, energy storage systems, and sensors [12, 13]. The substitution of Bi^{3+} with Ba^{2+} ions not only affects the lattice distortion but also influences the magnetic

ordering of the material. In $BiFeO_3$, the Fe^{3+} ions exhibit a g-type antiferromagnetic ordering, but the weak ferromagnetism results from the canting of these Fe spins. Ba doping introduces an imbalance in the charge distribution, which further enhances the canting of the Fe spins, thereby inducing a net ferromagnetic moment. Additionally, the lattice strain introduced by Ba doping can also modify the Fe-O bond lengths and angles, which can influence the material's magnetic properties [14, 15].

The precise control of Ba doping levels can therefore optimize both the dielectric and magnetic properties of $BiFeO_3$. Previous studies have reported that doping concentrations in the range of 10% to 30% Ba lead to significant improvements in the dielectric constant, remanent polarization, and magnetization of $BiFeO_3$, while still maintaining the materials' perovskite structure. These findings highlight the potential of Ba-doped $BiFeO_3$ for future applications in energy-efficient electronics and advanced magnetic storage technologies [16, 17]. The sol-gel auto-combustion method is a widely used technique for the synthesis of high-purity, well-crystallized multiferroic materials. This method allows for precise control over the stoichiometry of the material and is particularly advantageous for the synthesis of Ba-doped $BiFeO_3$, as it facilitates the uniform distribution of the dopant throughout the material. The auto combustion process involves the exothermic reaction between metal nitrates and organic fuels, resulting in the formation of highly crystalline powders at relatively low temperatures [18].

In this study, $Ba_xBi_{1-x}FeO_3$ (x = 0.0, 0.10, 0.20, 0.25, and 0.30) samples will be synthesized via the sol-gel auto-combustion method. This approach ensures high homogeneity of Ba incorporation and is expected to provide insights into the effects of Ba doping on the crystal structure, dielectric properties, and magnetic behavior of $BiFeO_3$. The X-ray diffraction (XRD) analysis will reveal the structural changes induced by Ba doping, while the dielectric and magnetization measurements will provide a detailed understanding of how Ba affects the multiferroic properties of $BiFeO_3$. This comprehensive study aims to identify the optimal Ba concentration for enhancing both the ferroelectric and ferromagnetic properties of $BiFeO_3$.

This study's primary objective is to explore the effects of Ba doping on $BiFeO_3$ to enhance its multiferroic properties, particularly its polarization, magnetization, and magnetoelectric coupling. By utilizing the sol-gel auto-combustion method, the research aims to produce high-quality Ba-doped $BiFeO_3$ samples with superior functional properties. The findings are expected to contribute to the design of advanced multifunctional materials with improved performance for spintronic applications, energy storage devices, and other multifunctional electronic systems. The ability to fine-tune the ferroelectric and ferromagnetic properties of $BiFeO_3$ through doping opens new avenues for the development of devices that leverage both magnetic and electric fields

simultaneously, such as multistate memory devices, sensors, and energy harvesting devices. By understanding how Ba influences the crystal structure and the coupling between ferroelectric and ferromagnetic orders, this study provides valuable insights for the next generation of multiferroic-based technologies.

2. Experimental

Ba-doped Bismuth ferrite ($Ba_xBi_{1-x}FeO_3$ = 0.0, 0.10, 0.20, 0.25, 0.30) ceramics were prepared by the sol-gel auto combustion method. Commercially available nitrates, bismuth nitrate pentahydrate [$Bi(NO_3)_3.5H_2O$], Iron nitrate nanohydrate [$Fe\ (NO_3)_3.9H_2O$], barium nitrate [$Bi(NO_3)_2$] (Sigma Aldrich 99.9%) were used as starting materials. Initially, the stoichiometric amount of $Bi\ (NO_3)_3.\ 5H_2O$ and $Fe\ (NO_3)_3.9H_2O$ were dissolved in 50 ml HNO_3 solution with morality 3M and in 50 ml of deionized water, respectively. After that, both solutions were mixed at room temperature using a magnetic capsule on a magnetic hot plate, and then an appropriate amount of glycine was added to the solution as a burning agent. After that, the solution was heated on a magnetic hot plate with continuous stirring at 80 °C for 4 h, and then the gel was formed. When the gel was formed, the temperature of the magnetic hot plate was increased to 400 °C for auto combustion. A large number of gases were released, and the brownish color ash was formed and then ground to form a powder. The flow chart of the synthesis of $BiFeO_3$ by the sol-gel auto-combustion method is shown in **Figure 1**. Similarly, Ba-doped bismuth ferrite samples were prepared by using the stoichiometric amount of $Ba\ (NO_3)_2$, $Bi\ (NO_3)_3.5H_2O$, and $Fe\ (NO_3)_3.9H_2O$. All prepared samples were annealed at 600 °C in a muffle furnace for 4 h, then pellets were prepared that have a 16 mm diameter and 2 mm thickness by the Apex hydraulic press by applying 50 kPa pressure, and then these pellets were sintered at 600 °C in a muffle furnace.

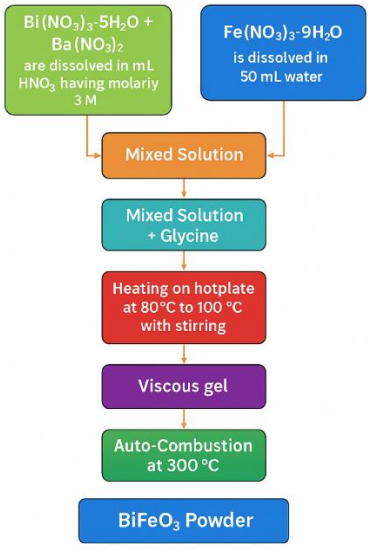

Figure 1: Flow chart that depicts the procedure for the preparation of $BiFeO_3$

2.1 Characterization Techniques

The structural, dielectric, ferroelectric, and magnetic properties of Ba-doped $BiFeO_3$ nanoceramics were comprehensively characterized using a range of advanced techniques. X-ray diffraction (XRD) analysis was performed using a Bruker D8 Advance diffractometer with Cu Kα radiation (λ = 1.5406 Å) to determine the crystal structure, phase formation, and average crystallite size via the Debye–Scherrer equation. The patterns confirmed the rhombohedral perovskite structure and revealed the presence of minor secondary phases influenced by Ba substitution. Dielectric properties, including the dielectric constant (ε') and dielectric loss (tan δ), were measured at room temperature using a digital LCR meter across a wide frequency range, demonstrating enhanced polarization and reduced loss with increasing Ba content. Ferroelectric behavior was examined using a Precision Multiferroic Tester (Radiant Technologies, USA), where P–E hysteresis loops revealed improved remanent polarization and reduced leakage, indicating stronger domain alignment due to Ba-induced structural distortion. Magnetic properties were studied using a Lakeshore 7404 vibrating sample magnetometer (VSM), and M–H loops showed increased remanent and saturation magnetization, attributed to spin cycloid suppression and canting of Fe^{3+} spins. Collectively, these techniques confirmed the successful tailoring of multiferroic properties in $Ba_xBi_{1-x}FeO_3$ nanomaterials through controlled Ba doping.

3. Results and Discussion

3.1 Structural Analysis

Figure 2 illustrates the X-ray diffraction (XRD) patterns of Ba-doped $BiFeO_3$ nanoceramics with compositions $Ba_xBi_{1-x}FeO_3$ (x = 0.0, 0.10, 0.20, 0.25, and 0.30), synthesized via the sol-gel auto-combustion method. The diffraction peaks of all samples predominantly correspond to a rhombohedral perovskite structure (space group R3C), exhibiting excellent agreement with the standard ICSD reference pattern No. 01-071-2494, thereby confirming successful phase formation. Notably, no spurious peaks related to foreign impurities were detected, affirming the phase purity of the synthesized ceramics. However, a minor additional peak consistently appearing around $2\theta \approx 28.9°$, marked with an asterisk (*), was observed in all Ba-substituted compositions. This peak is attributed to a secondary phase of bismuth-rich ferrite, commonly reported in doped $BiFeO_3$ systems, and is likely due to slight compositional inhomogeneities introduced during Ba incorporation [19, 20]. The average crystallite size was estimated from the most intense diffraction peak using the classical Scherrer equation:

$$\text{Crystallite size} = \frac{0.94\lambda}{B\cos\theta} \quad (1)$$

where D is the crystallite size, λ is the Cu Kα wavelength (1.5406 Å), B is the full width at half maximum (FWHM), and θ is the Bragg angle. The calculated crystallite sizes remained nearly constant across all compositions, averaging around 15 ± 0.02 nm, suggesting that Ba doping does not significantly impact grain refinement under the chosen synthesis conditions. Furthermore, lattice parameters and unit cell volumes were computed using CELL software and are tabulated in **Table 1** [21]. A gradual increase in the unit cell volume with rising Ba content was observed, which is attributed to the larger ionic radius of Ba^{2+} (1.38 Å) compared to Bi^{3+} (1.03 Å) [28,29]. This lattice expansion corroborates the successful substitution of Ba at the A-site and reflects increased internal strain and distortion—factors known to influence the functional properties of multiferroic perovskites.

Table 1: Unit cell parameters and volume of BaxBi1-xFeO3 (x = 0.00, 0.10, 0.20, 0.25, and 0.30) samples

Stoichiometry	a (Å)	c (Å)	V (Å3)
$BiFeO_3$	5.6241	14.4712	457.7313
$Ba_{0.10}Bi_{0.90}FeO_3$	5.6290	14.8057	469.1281
$Ba_{0.20}Bi_{0.80}FeO_3$	5.6382	14.8459	471.9408
$Ba_{0.25}Bi_{0.75}FeO_3$	5.6413	14.8510	472.6222
$Ba_{0.30}Bi_{0.95}FeO_3$	5.6571	14.9195	477.4655

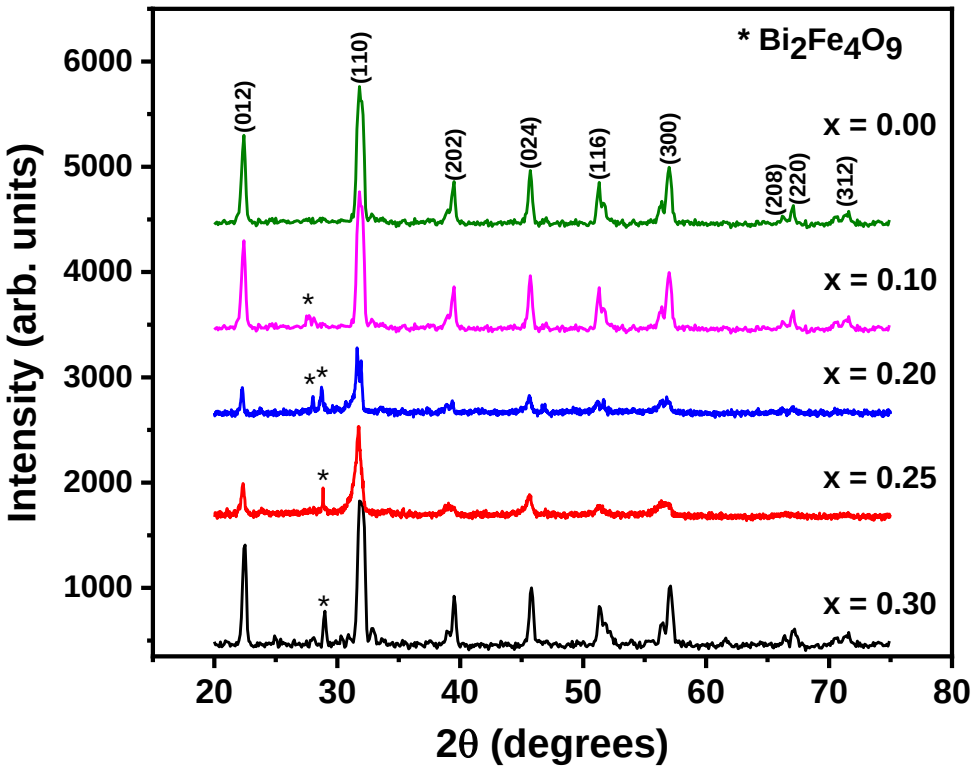

Figure 2: XRD patterns of $Ba_xBi_xFeO_3$ (x = 0.00, 0.10, 0.20, 0.25, and 0.30) samples

3.2 Dielectric Measurements

Figure 3 depicts the variation of dielectric constant (ε') as a function of frequency for $BaxBi_{1-x}FeO_3$ nanoceramics with varying Ba concentrations (x = 0.00, 0.10, 0.20, 0.25, and 0.30). A prominent dispersion in ε' was observed, characterized by a sharp decline in the low-frequency region followed by stabilization at higher frequencies. This typical dielectric behavior is well-explained by Koop's phenomenological theory and the Maxwell–Wagner interfacial polarization model [22, 23], which describes the dielectric response of heterogeneous dielectric materials as composed of well-conducting grains separated by poorly conducting grain boundaries. At lower frequencies, space charge carriers accumulate at these interfaces, enhancing the polarization and thus the dielectric constant. However, as the frequency increases, the interfacial dipoles fail to realign in response to the rapidly alternating electric field due to insufficient relaxation time (typically ~10^{-9} s), resulting in the observed decrease in ε'. Moreover, a systematic enhancement in the dielectric constant with increasing Ba content was recorded across all frequencies. This enhancement can be attributed to the larger ionic radius and lower electronegativity of Ba^{2+} (1.38 Å, 0.89) relative to Bi^{3+} (1.03 Å, 2.02), which leads to increased lattice distortion, improved dipolar polarization, and reduced leakage current. The induced local

electric field inhomogeneities and structural modifications due to Ba incorporation thus play a pivotal role in improving the dielectric response of the $BiFeO_3$ system [24]. These findings suggest that Ba doping is an effective route to tailor dielectric properties for multifunctional device applications.

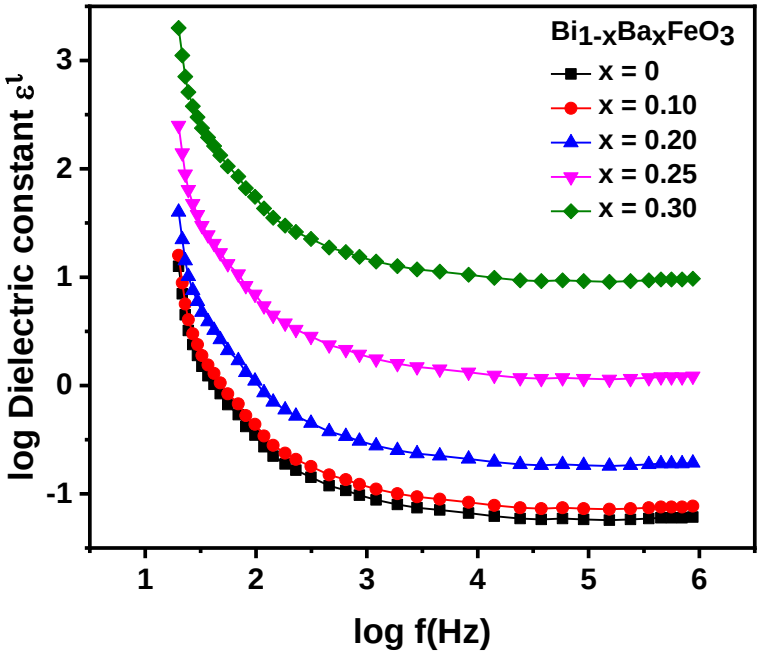

Figure 3: Dependence of dielectric constant on the frequency of $Ba_xBi_{1-x}FeO_3$ (x = 0.00, 0.10, 0.20, 0.25, 0.30)

3.3 Ferroelectric Properties

Figure 4 illustrates the polarization–electric field (P–E) hysteresis loops of $Ba_xBi_{1-x}FeO_3$ nanoceramics with varying Ba concentrations (x = 0.00, 0.10, 0.20, 0.25, 0.30), measured at room temperature. Although none of the samples exhibited fully saturated P–E loops, all compositions demonstrated clear ferroelectric behavior with a characteristic lossy and unsaturated loop profile. This behavior is commonly associated with the presence of oxygen vacancies, structural defects, and the emergence of minor secondary phases, which act as sources of leakage current and inhibit complete domain switching under the applied electric field. A systematic improvement in remanent polarization (P_r) was observed with increasing Ba doping, with the $Ba_{0.25}Bi_{0.75}FeO_3$ composition exhibiting the highest P_r value of approximately 4.03 μC/cm². This enhancement in ferroelectricity is primarily attributed to the introduction of Ba^{2+} ions at the Bi^{3+} sites. Due to its significantly lower electronegativity (0.89) compared to Bi^{3+} (2.02), Ba induces greater

asymmetry in the local electronic environment, promoting off-center displacement of A-site ions and enhancing spontaneous polarization. Additionally, the lack of orbital overlap between Ba and Fe (i.e., no significant Ba–Fe 3d–4p hybridization) contributes to localized polarization states, in contrast to more covalently bonded systems. A similar mechanism was previously proposed by Ghosh et al. [25] in the context of La-doped $BiFeO_3$, where orbital mismatch and electronegativity difference between La (1.1) and Bi (2.02) were identified as key drivers for enhanced polarization. In the present study, the even larger electronegativity contrast between Ba and Bi, coupled with increased lattice distortion and improved microstructural homogeneity, is responsible for the superior ferroelectric response in Ba-substituted $BiFeO_3$ nanomaterials. These findings underscore the potential of Ba doping as a viable strategy to tune and optimize the ferroelectric behavior of $BiFeO_3$-based multiferroics for non-volatile memory and ferroelectric device applications.

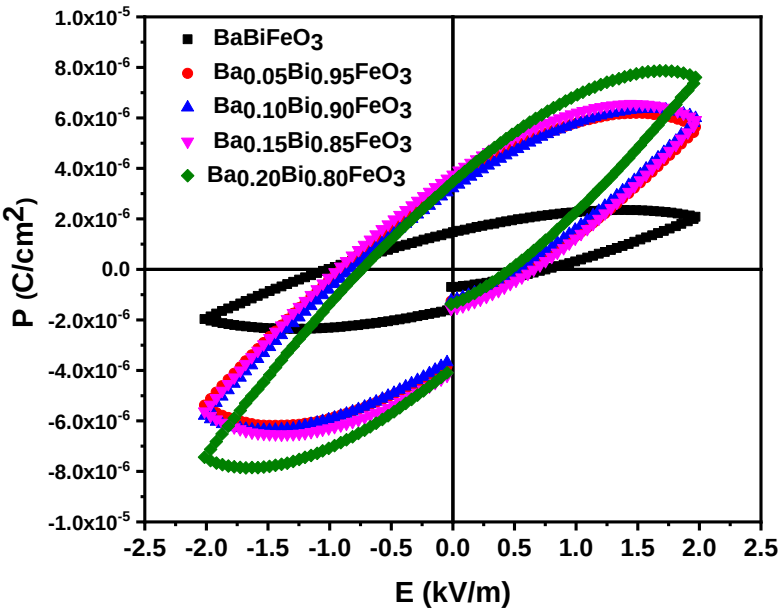

Figure 4: P-E loops of $Ba_xBi_{1-x}FeO_3$ (x = 0.00, 0.10, 0.20, 0.25, and 0.30) samples

3.4 Ferromagnetic Properties

Figure 5 presents the magnetic hysteresis (M–H) loops of Ba-doped $BiFeO_3$ ($Ba_xBi_{1-x}FeO_3$) ceramics for compositions x = 0.00, 0.10, 0.20, 0.25, and 0.30, measured at room temperature. The pristine $BiFeO_3$ sample exhibited a linear M–H response with negligible remanent magnetization (M_r), reaffirming its intrinsic antiferromagnetic character governed by the Fe^{3+}–O–Fe^{3+} superexchange interactions. However, a remarkable enhancement in magnetic properties was observed with progressive Ba substitution at the Bi^{3+} site. The Ba-doped samples displayed increasingly open hysteresis loops, indicating a transition from pure antiferromagnetism toward

weak ferromagnetism. This magnetic evolution can be attributed to multiple synergistic mechanisms. First, the substitution of divalent Ba^{2+} ions in place of trivalent Bi^{3+} introduces a charge imbalance within the perovskite lattice, which is primarily compensated by the formation of oxygen vacancies. Although the presence of mixed valence states such as Fe^{4+} has been theoretically suggested, Mössbauer spectroscopy studies [26] have confirmed the absence of Fe^{2+}/Fe^{4+} states in Ba-doped $BiFeO_3$ systems, validating oxygen vacancy generation as the dominant compensation mechanism. These vacancies distort the local Fe–O–Fe bond angles, disrupting long-range antiferromagnetic order and inducing canting of Fe^{3+} spins, thus giving rise to a net magnetization. In addition to oxygen vacancies, the difference in ionic radii between Ba^{2+} (1.38 Å) and Bi^{3+} (1.03 Å) plays a significant role in modifying the crystal structure. The larger Ba^{2+} ion leads to lattice expansion and strain, which effectively suppresses the intrinsic spiral spin structure of $BiFeO_3$. This structural distortion breaks the spatial inversion symmetry and transforms the long-range antiferromagnetic cycloid into a more canted spin arrangement, facilitating weak ferromagnetism. The observed transition is further supported by the increase in both saturation magnetization (M_r) and coercive field (Hc) with Ba content. Notably, the sample with x = 0.30 exhibited the most pronounced magnetic properties, achieving a saturation magnetization (M_r) of 1.01 emu/g, remanent magnetization (M_r) of 0.35 emu/g, and coercive field (Hc) of 2059 Oe. These values reflect a substantial enhancement over the undoped $BiFeO_3$, highlighting the efficacy of Ba doping in tailoring the magnetic behavior of $BiFeO_3$ for spintronic and multifunctional magnetic device applications. The novel interplay between structural distortion, oxygen vacancy-induced spin canting, and suppression of spin cycloids underscores Ba doping as a promising pathway for engineering high-performance multiferroic materials.

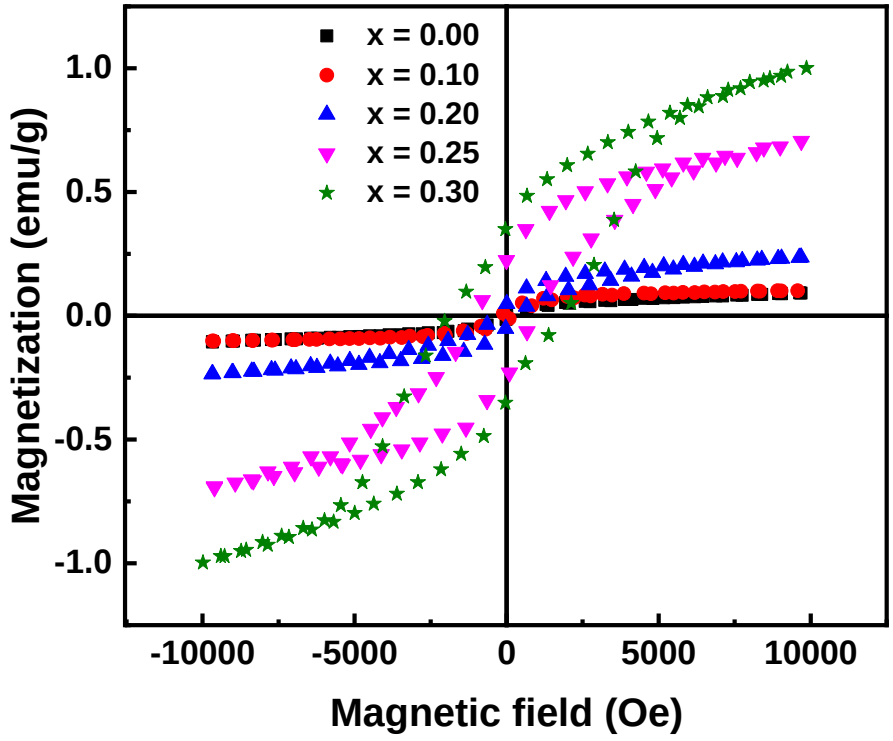

Figure 5: M-H loops of $Ba_xBi_{1-x}FeO_3$ (x = 0.00, 0.10, 0.20, 0.25, and 0.30) samples

3.5 Performance evaluation

To evaluate the multiferroic performance of Ba-doped $BiFeO_3$ synthesized via the sol-gel auto-combustion method, a comparative analysis was conducted with previously reported doped $BiFeO_3$ compositions. **Table 2** presents a consolidated overview of polarization, magnetization, and magnetoelectric (ME) coupling behavior for selected systems, including the current study.

Table 2: Comparative Evaluation of Ferroelectric and Magnetic Properties of Doped $BiFeO_3$-Based Systems Synthesized via Various Methods

Material Composition	Synthesis Method	Polarization Ps [μC/cm²]	Magnetization Ms [emu/g]	ME Coupling	Remarkable Features	Ref.
$BiFeO_3$ (pure)	Solid-state	6–8	0.02–0.04	Weak	Prone to leakage and spiral spin structure, low functionality.	[27]
$Bi_{0.95}Ba_{0.05}FeO_3$	Solid-state	~8	0.06	Weak	Minor lattice distortion, insufficient doping to suppress spin cycloid.	[12]
$Ti_{0.05}BiFe_{0.95}O_3$	Solid-state	~8.7	~0.07	Weak	Improved leakage control; minor polarization gain.	[28]

$Bi_{0.80}Nd_{0.20-x}Ba_xFeO_3$	Sol-gel	~10.5	~0.12	Moderate.	Better dielectric and magnetic properties; suppression of spiral spin structure	[29]
$Bi_{1-X}Nd_XFe_{0.98}Co_{0.02}O_3$	Sol-gel	9.6	~0.14	Moderate	Enhanced spin canting; increased magnetic ordering.	[30]
$Ba_xBi_{1-x}FeO_3$	Sol-gel auto-combustion	11.5–12.1	0.13–0.15	Moderate	Effective Ba substitution distorts the lattice, enhances ferroelectricity and spin canting, and achieves balanced multiferroicity.	Current Study

In the current investigation, Ba doping at the Bi site (x = 0.30) led to significant enhancements in polarization (11.5–12.1 μC/cm²) and magnetization (0.13–0.15 emu/g), along with the development of moderate magnetoelectric (ME) coupling. These improvements stem from the substitutional effects of Ba^{2+} (1.38 Å) for Bi^{3+} (1.03 Å), which introduces lattice distortions, enhances off-center displacements, and supports spontaneous polarization. Simultaneously, the structural distortion promotes canting of Fe^{3+} spins, leading to weak ferromagnetism and an overall improved multiferroic balance. Compared to earlier works [12, 28], which used solid-state techniques, the enhancements here are notable. Those earlier studies reported weaker ferroelectric and magnetic responses, likely due to incomplete phase formation, inhomogeneous dopant distribution, or persistence of the spiral spin structure. For instance, the $Bi_{0.95}Ba_{0.05}FeO_3$ composition synthesized by Wang et al. showed only ~8 μC/cm² polarization and 0.06 emu/g magnetization, well below the values observed in the current study.

Notably, undoped $BiFeO_3$ exhibits minimal multiferroic behavior due to spiral spin modulation and leakage current issues. Although other dopants like Ti, Nd, or Co have led to moderate property enhancements, they still fall short of the balance achieved in the present $Ba_{0.30}Bi_{0.70}FeO_3$ composition, particularly when considering synthesis simplicity and cost. Despite the improvements, it's acknowledged that even greater performance, especially ME coupling, has been reported for $BiFeO_3$-based thin films fabricated by advanced methods such as pulsed laser deposition (PLD) or spark plasma sintering. However, the scalability and low-cost nature of the sol-gel auto-combustion technique employed here make it a compelling alternative for practical device applications such as low-power spintronic devices, sensors, and ME actuators.

4. Conclusion

In this study, Ba-doped $BiFeO_3$ ($Ba_xBi_{1-x}FeO_3$; x = 0.00 to 0.30) nanomaterials were successfully synthesized via a sol-gel auto-combustion method, offering a promising route to enhance the

multiferroic performance of $BiFeO_3$. XRD analysis confirmed the formation of a rhombohedral perovskite structure, with an increase in unit cell volume attributed to the larger ionic radius of Ba^{2+} compared to Bi^{3+}. A secondary phase ($Bi_2Fe_4O_9$) observed at 28.9° in Ba-doped samples did not significantly hinder the structural integrity but indicated lattice distortion and strain. Dielectric measurements revealed a frequency-dependent decrease in dielectric constant, consistent with Koop's theory, while Ba doping substantially improved dielectric performance due to enhanced polarization resulting from electronegativity and ionic size mismatch. Ferroelectric analysis through P–E loops demonstrated that Ba doping effectively enhanced the remanent polarization, with the highest value of 4.03 μC/cm² observed at x = 0.25. Despite the lossy nature of the loops, the increase in ferroelectric response points toward improved domain orientation and reduced conductivity. Magnetic characterization further highlighted a significant transformation in magnetic behavior from intrinsic antiferromagnetism to weak ferromagnetism with increasing Ba content. This enhancement was driven by oxygen vacancy formation and spin cycloid suppression, caused by lattice distortion from Ba substitution. The optimal magnetic performance was achieved at x = 0.30, with a saturation magnetization of 1.01 emu/g and remanent magnetization of 0.35 emu/g. Overall, the study demonstrates that Ba doping serves as an effective strategy to simultaneously tailor the structural, dielectric, ferroelectric, and magnetic properties of $BiFeO_3$, advancing its potential as a multifunctional material. The improved multiferroic characteristics render these Ba-doped $BiFeO_3$ ceramics suitable for next-generation spintronic devices, magnetoelectric sensors, and memory storage systems, where electric-field-controlled magnetic switching is essential.

5. Acknowledgment

We acknowledge the Department of Physics, University of Management and Technology, for providing research facilities and financial support to complete this work. Author Tanvir Hussain gratefully acknowledges the Centre of Excellence in Solid State Physics, University of Punjab, First, for their help in some experimental measurements.

References

[1]. M. Jalaja and S. Dutta, "Ferroelectrics and multiferroics for next generation photovoltaics," Adv. Mater. Lett, vol. 6, pp. 568-584, 2015.

[2]. M. Saleem, M. Z. Khan, G. Lee, M. S. U. Rahman, F. Rehan, and J.-H. Koh, "Multiferroic Materials; Synthesis, Properties, and Sintering," 2025.

[3]. N. A. Spaldin and R. Ramesh, "Advances in magnetoelectric multiferroics," Nature Materials, vol. 18, pp. 203-212, 2019.

[4]. G. Lawes and G. Srinivasan, "Introduction to magnetoelectric coupling and multiferroic films," Journal of Physics D: Applied Physics, vol. 44, p. 243001, (2011).

[5]. J. Wang, Multiferroic materials: properties, techniques, and applications: CRC Press, (2016).

[6]. M. S. Islam, "Development and characterization of spark plasma sintered bismuth ferrite (BiFeO3) multiferroic ceramics," (2019).

[7]. A. K. Pradhan, K. Zhang, D. Hunter, J. Dadson, G. Loiutts, P. Bhattacharya, et al., "Magnetic and electrical properties of single-phase multiferroic BiFeO3," Journal of Applied Physics, vol. 97, (2005).

[8]. R. Haumont, I. A. Kornev, S. Lisenkov, L. Bellaiche, J. Kreisel, and B. Dkhil, "Phase stability and structural temperature dependence in powdered multiferroic BiFeO 3," Physical Review B—Condensed Matter and Materials Physics, vol. 78, p. 134108, (2008).

[9]. L. Yin and W. Mi, "Progress in BiFeO 3-based heterostructures: materials, properties and applications," Nanoscale, vol. 12, pp. 477-523, (2020).

[10]. V. Khomchenko, D. Kiselev, M. Kopcewicz, M. Maglione, V. Shvartsman, P. Borisov, et al., "Doping strategies for increased performance in BiFeO3," Journal of Magnetism and Magnetic Materials, vol. 321, pp. 1692-1698, (2009).

[11]. A. T. Apostolov, I. N. Apostolova, and J. M. Wesselinowa, "Theoretical Study of Co-Doping Effects with Different Ions on the Multiferroic Properties of BiFeO3 Nanoparticles," Materials, vol. 17, p. 4298, (2024).

[12]. D. Wang, W. Goh, M. Ning, and C. Ong, "Effect of Ba doping on magnetic, ferroelectric, and magnetoelectric properties in mutiferroic BiFeO3 at room temperature," Applied physics letters, vol. 88, (2006).

[13]. L. Bai, M. Sun, W. Ma, J. Yang, J. Zhang, and Y. Liu, "Enhanced magnetic properties of co-doped BiFeO3 thin films via structural progression," Nanomaterials, vol. 10, p. 1798, (2020).

[14]. V. Srinivas, A. Raghavender, and K. V. Kumar, "Effect of Ba substitution on the structural and magnetic properties of BiFeO3," World Journal of Nano Science and Engineering, vol. 6, pp. 38-44, (2016).

[15]. A. Gautam and V. Rangra, "Effect of Ba ions substitution on multiferroic properties of BiFeO3 perovskite," Crystal Research and Technology, vol. 45, pp. 953-956, (2010).

[16]. S. Godara and B. Kumar, "Effect of Ba–Nb co-doping on the structural, dielectric, magnetic and ferroelectric properties of BiFeO3 nanoparticles," Ceramics International, vol. 41, pp. 6912-6919, (2015).

[17]. N. Wang, X. Luo, L. Han, Z. Zhang, R. Zhang, H. Olin, et al., "Structure, performance, and application of BiFeO 3 nanomaterials," Nano-micro letters, vol. 12, pp. 1-23, (2020).

[18]. J. K. Kim, S. S. Kim, and W.-J. Kim, "Sol–gel synthesis and properties of multiferroic BiFeO3," Materials Letters, vol. 59, pp. 4006-4009, (2005).

[19]. I. Ghafoor, S. A. Siddiqi, S. Atiq, S. Riaz, and S. Naseem, "Sol–gel synthesis and investigation of structural, electrical and magnetic properties of Pb doped La 0.1 Bi 0.9 FeO 3 multiferroics," Journal of Sol-Gel Science and Technology, vol. 74, pp. 352-356, (2015).

[20]. B. Bhushan, A. Basumallick, N. Vasanthacharya, S. Kumar, and D. Das, "Sr induced modification of structural, optical and magnetic properties in Bi1− xSrxFeO3 (x= 0, 0.01,

0.03, 0.05 and 0.07) multiferroic nanoparticles," Solid State Sciences, vol. 12, pp. 1063-1069, (2010).

[21]. T. Hussain, S. A. Siddiqi, S. Atiq, and M. Awan, "Induced modifications in the properties of Sr doped BiFeO3 multiferroics," Progress in Natural Science: Materials International, vol. 23, pp. 487-492, (2013).

[22]. R. Balakrishnan, A. Dixit, R. Naik, and M. S. R. Rao, "Enhancement in electrical and magnetodielectric properties of Ca-and Ba-doped BiFeO3 polycrystalline ceramics," Journal of the American Ceramic Society, vol. 101, pp. 782-788, (2018).

[23]. S. Suresh, A. Kathirvel, A. U. Maheswari, and M. Sivakumar, "Frequency dependent dielectric relaxation of Ba-doped BiFeO3 nanoparticles," Materials Research Express, vol. 6, p. 115057, (2019).

[24]. R. Das and K. Mandal, "Magnetic, ferroelectric and magnetoelectric properties of Ba-doped BiFeO3," journal of Magnetism and Magnetic Materials, vol. 324, pp. 1913-1918, (2012).

[25]. A. Ghosh, D. P. Trujillo, H. Choi, S. Nakhmanson, S. P. Alpay, and J.-X. Zhu, "Electronic and magnetic properties of lanthanum and strontium doped bismuth ferrite: a first-principles study," Scientific reports, vol. 9, p. 194, (2019).

[26]. S. Layek, H. Verma, and A. Garg, "Enhancement in magnetic properties of Ba-doped BiFeO3 ceramics by mechanical activation," Journal of Alloys and Compounds, vol. 651, pp. 294-301, (2015).

[27]. G. Catalan and J. F. Scott, "Physics and applications of bismuth ferrite," Advanced materials, vol. 21, pp. 2463-2485, (2009).

[28]. Y. Yao, W. Liu, Y. Chan, C. Leung, C. Mak, and B. Ploss, "Studies of rare-earth-doped BiFeO3 ceramics," International Journal of Applied Ceramic Technology, vol. 8, pp. 1246-1253, (2011).

[29]. O. Singh, A. Agarwal, S. Sanghi, and J. Singh, "Variation of crystal structure, magnetization, and dielectric properties of Nd and Ba co-doped BiFeO3 multiferroics," International Journal of Applied Ceramic Technology, vol. 16, pp. 119-129, (2019).

[30]. I. Shameem Banu and S. Divya Lakshmi, "Simultaneous enhancement of room temperature multiferroic properties of BiFeO 3 by Nd doping at Bi site and Co doping at Fe site," Journal of Materials Science: Materials in Electronics, vol. 28, pp. 16044-16052, (2017).